Molecular-rotation-induced modulation of the tunneling dissociation time delay in H_2^+

Junping Wang [1,2,3] Feng He [4] Jian Wu,[2,3,5] and Hongcheng Ni [2,5,*]

[1]*College of Physics, Liaoning University, Liaoning, Shenyang 110036, China*

[2]*State Key Laboratory of Precision Spectroscopy, East China Normal University, Shanghai 200241, China*

[3]*Chongqing Key Laboratory of Precision Optics, Chongqing Institute of East China Normal University, Chongqing 401121, China*

[4]*Key Laboratory for Laser Plasmas (Ministry of Education) and School of Physics and Astronomy, Collaborative Innovation Center for IFSA, Shanghai Jiao Tong University, Shanghai 200240, China*

[5]*Collaborative Innovation Center of Extreme Optics, Shanxi University, Taiyuan, Shanxi 030006, China*

(Received 25 November 2025; accepted 6 March 2026; published 24 March 2026)

The question of whether quantum tunneling imposes a finite time delay is a fundamental and contested issue, prominently debated in strong-field atomic ionization. Here we extend this debate to the molecular domain by investigating the tunneling dissociation time of the proton in H_2^+. Through numerical solution of a two-level time-dependent Schrödinger equation and analysis via the backpropagation method, we discover a significant and tunable delay in the proton's emergence. Crucially, we demonstrate that this delay is not intrinsic but is primarily governed by the relative timescales of two motions. The delay's sign is determined by the competition between the laser cycle and the molecular rotational period: It is positive when the laser cycle is shorter than half the rotational period and negative in the opposite regime. Our work underlines the importance of tunneling dissociation delay by revealing its physical origin, establishing laser-driven molecular rotation as a powerful control knob and tunneling delay as a real-time probe of ultrafast rotational dynamics.

DOI: 10.1103/k8dk-y5pc

I. INTRODUCTION

The question of whether quantum tunneling requires finite time has been a subject of intense debate since the early days of quantum mechanics [1–7]. The advent of the attoclock technique [8] has enabled direct measurements of tunneling time delays, yet their interpretation remains contentious, giving rise to two conflicting viewpoints. One asserts a negligible or even vanishing time delay during tunneling [9–20], while the other reports finite positive delays [21–28]. Early attoclock experiments on helium suggested negligible delays [9], while controversy was further intensified by subsequent studies insisting on the existence of finite delays [21]. The single-electron nature of atomic hydrogen makes it an ideal system to isolate pure tunneling dynamics. A landmark study by Sainadh *et al.* [17] combined the attoclock technique with Yukawa-potential simulations, concluding that apparent delays originate not from tunneling itself, but from post-tunneling interactions with the ionic core. This perspective, however, is challenged by findings in diverse systems. Experiments with cold atoms have reported tunneling times on the millisecond scale [28], and theoretical work suggests that proton tunneling in DNA and ion tunneling in G-quadruplex structures occur with picosecond-scale delays [29,30]. These findings underscore a central insight: The existence of a finite tunneling time delay is highly dependent on the specific system and the measurement conditions.

Molecular dissociation in laser fields provides a distinct paradigm for probing tunneling dynamics. Tunneling dissociation is increasingly recognized for its role in chemical transformations, with the capacity to fundamentally alter reaction pathways [31], enable coherent control of chemical reactions [32], and facilitate novel modes of reactivity [33]. As the simplest molecular system, the H_2^+ molecular ion and its isotopes serve as fundamental benchmarks for studying ultrafast dissociation mechanisms [34–38], with pronounced isotopic effects further allowing for precise tracking of nuclear-wave-packet dynamics [39,40]. Over decades, synergistic theoretical and experimental efforts have identified a rich variety of dissociation pathways in short-wavelength lasers, including bond softening [34], bond hardening [35], above-threshold dissociation [36], and rescattering-induced breakup [37].

In long-wavelength laser fields, suppressed potential barriers allow high-lying vibrational states to undergo over-barrier dissociation. Classical trajectory and wave-packet dynamics studies have revealed rich phenomena such as dynamical dissociation quenching and laser-controlled dissociation [41–47]. In contrast, tunneling dissociation, which occurs when the vibrational energy lies below the laser-dressed barrier, has been far less explored, largely due to the experimental challenge of observing it with current laser technologies. Up to now, evidence has been reported in systems such as Ar_2^+ [46] and $dd\mu$ molecules [48] and more recently tunneling dissociation of NH_4^+ was observed in a cryogenic ion trap with a millisecond-scale lifetime [49].

For the simplest molecular ion H_2^+ and its isotopes, Li *et al.* [38] provided evidence of tunneling dissociation

*Contact author: hcni@lps.ecnu.edu.cn

under a linearly polarized terahertz field via vibrational-state-dependent dissociation probabilities. Very recently, Tian *et al.* [50] investigated proton tunneling in H_2^+ and its asymmetric isotopologues HD^+ and HT^+ driven by a circularly polarized terahertz laser field, revealing that the angular distribution of emitted protons is modulated by molecular alignment and rotation. Despite these advances, key ultrafast dynamical characteristics, such as the dissociation time delay, spatial origin of the dissociating wave packet, and its momentum distribution at the tunnel exit, remain unexplored, which are essential for a complete understanding of the tunneling dissociation process.

In this work we report a numerical investigation of the tunneling dissociation of H_2^+ by solving the two-level time-dependent Schrödinger equation (TDSE). To unambiguously resolve the tunneling dynamics and to avoid the complication of nuclear-wave-packet recollision inherent in linearly polarized fields, we employ a circularly polarized terahertz field. This choice not only ensures the isolation of individual tunneling events akin to the attoclock technique in atomic ionization but also introduces the capability to actively control molecular rotation via the field's continuous torque. We extend the backpropagation method [7,12,51,52], originally developed for atomic tunneling ionization, to molecular tunneling dissociation. This approach allows us to quantitatively examine key, previously inaccessible parameters of the tunneling dissociation process, including the dissociation time, the exit position, and the nuclear momentum distribution at the tunnel exit, thereby providing a complete spatiotemporal picture of the tunneling dissociation dynamics.

This paper is structured as follows. In Sec. II we detail the model for the tunneling dissociation of H_2^+ used in our study. In Sec. III we present our findings and discuss their physical origins. A summary and conclusions are provided in Sec. IV. Atomic units are used throughout unless stated otherwise.

II. MODEL FOR TUNNELING DISSOCIATION OF H_2^+

Within the Born-Oppenheimer approximation, the wave function of H_2^+ can be expressed in terms of the two lowest electronic states as

$$\Psi(\boldsymbol{r},\boldsymbol{R};t)=\chi_g(\boldsymbol{R},t)\phi_g(\boldsymbol{r},\boldsymbol{R})+\chi_u(\boldsymbol{R},t)\phi_u(\boldsymbol{r},\boldsymbol{R}), \quad (1)$$

where $\boldsymbol{r}$ denotes the electronic coordinate, $\boldsymbol{R}$ represents the internuclear displacement, and $\phi_g(\mathbf{r},\boldsymbol{R})$ and $\phi_u(\boldsymbol{r},\boldsymbol{R})$ correspond to the orthogonal $1s\sigma_g$ and $2p\sigma_u$ electronic states, respectively. Other highly excited electronic states are neglected as they lie significantly higher in the energy diagram and couple only weakly with the two lowest states under our laser parameters. The time evolution of the nuclear rovibrational wave functions $\chi_g(\boldsymbol{R},t)$ and $\chi_u(\boldsymbol{R},t)$, associated with the ground and first excited electronic states, is governed by the TDSE [50,53–59]

$$i\frac{\partial}{\partial t}\begin{pmatrix}\chi_g(\boldsymbol{R},t)\\ \chi_u(\boldsymbol{R},t)\end{pmatrix}=(H_0+H_I)\begin{pmatrix}\chi_g(\boldsymbol{R},t)\\ \chi_u(\boldsymbol{R},t)\end{pmatrix}, \quad (2)$$

where the field-free Hamiltonian

$$H_0=\begin{pmatrix}\frac{\boldsymbol{P}^2}{2\mu}+V_g(\boldsymbol{R}) & 0\\ 0 & \frac{\boldsymbol{P}^2}{2\mu}+V_u(\boldsymbol{R})\end{pmatrix}, \quad (3)$$

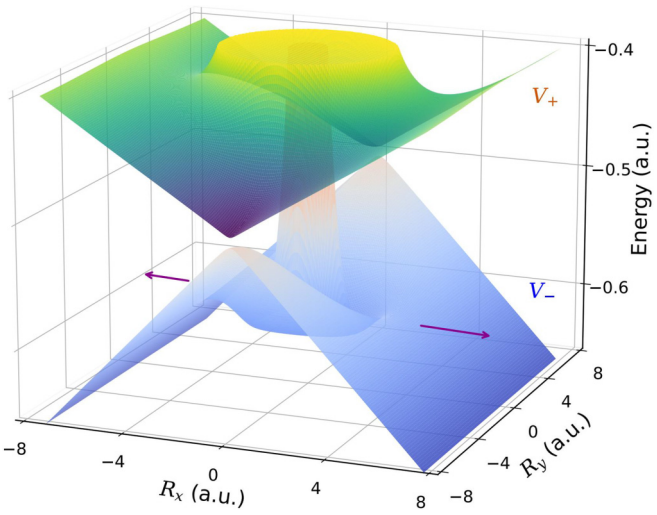

FIG. 1. Field-dressed quasistatic potential energy surface $V_\pm$ of H_2^+. The purple arrows indicate the tunneling dissociation channels through the potential barriers when the electric field is aligned along the x axis. The laser intensity used is 1.3×10^{14} W/cm^2.

where $\mu=918$ a.u. is the reduced nuclear mass of H_2^+, $\boldsymbol{P}$ is the momentum operator, and $V_g(\boldsymbol{R})$ and $V_u(\boldsymbol{R})$ are the isotropic Born-Oppenheimer potential energy surfaces for the $1s\sigma_g$ and $2p\sigma_u$ states [60], respectively. The laser-molecule interaction Hamiltonian in the dipole approximation and length gauge is

$$H_I=\begin{pmatrix}0 & \boldsymbol{F}(t)\cdot\boldsymbol{D}(\boldsymbol{R})\\ \boldsymbol{F}(t)\cdot\boldsymbol{D}(\boldsymbol{R}) & 0\end{pmatrix}, \quad (4)$$

with $\boldsymbol{D}(\boldsymbol{R})$ the transition dipole moment between the $1s\sigma_g$ and $2p\sigma_u$ electronic states [61] and $\boldsymbol{F}(t)$ the laser electric field given by

$$\boldsymbol{F}(t)=F_0\cos^4\left(\frac{\omega t}{2N}\right)[\cos(\omega t)\hat{\boldsymbol{e}}_x+\sin(\omega t)\hat{\boldsymbol{e}}_y], \quad (5)$$

where F_0 represents the field amplitude, ω denotes the angular frequency, and N is the number of optical cycles.

For long-wavelength fields, we adopt the adiabatic representation to analyze dissociation pathways [56,57,62]. The instantaneous potentials $V_\pm$ and eigenstates $\chi_\pm$ are

$$V_\pm(\boldsymbol{R},t)=\frac{V_g(\boldsymbol{R})+V_u(\boldsymbol{R})}{2}\pm\sqrt{\frac{[V_g(\boldsymbol{R})-V_u(\boldsymbol{R})]^2}{4}+[\boldsymbol{F}(t)\cdot\boldsymbol{D}(\boldsymbol{R})]^2}, \quad (6)$$

$$\chi_-(\boldsymbol{R},t)=\cos(\alpha)\chi_g(\boldsymbol{R},t)+\sin(\alpha)\chi_u(\boldsymbol{R},t), \quad (7)$$

$$\chi_+(\boldsymbol{R},t)=-\sin(\alpha)\chi_g(\boldsymbol{R},t)+\cos(\alpha)\chi_u(\boldsymbol{R},t), \quad (8)$$

with

$$\tan(2\alpha)=-2\frac{\boldsymbol{F}(t)\cdot\boldsymbol{D}(\boldsymbol{R})}{V_g(\boldsymbol{R})-V_u(\boldsymbol{R})}. \quad (9)$$

The field-dressed potential energy surface $V_\pm$ of H_2^+ is shown in Fig. 1. It can be seen that the $1s\sigma_g$ potential energy surface is bent under the influence of the external field, forming a potential barrier with finite height along the field direction, denoted by V_-. In this case, if the electric

field changes slowly enough compared to the nuclear motion, the nuclear wave packet may tunnel through this barrier, as indicated by the purple arrows in Fig. 1.

The isotropic initial rovibrational state is obtained numerically through imaginary-time propagation [63], and the subsequent wave function evolution is performed by solving the TDSE in the diabatic representation using the Crank-Nicolson method [64]. It is worth noting that, in order to analyze the tunneling dissociation process, the dissociated part of the wave function is examined in the adiabatic representation after the propagation. Our simulations focus on nuclear dynamics within the laser polarization plane (x, y), as wave-packet expansion along the laser propagation direction presents no significant physical complexity. The computational parameters are optimized as spatial steps $\Delta R_x = \Delta R_y = 0.02$ a.u. and temporal steps $\Delta t = 0.1$ a.u., with convergence verified through grid refinement tests. The simulation domain extends to $R_{\max} = 50$ a.u. in both the x and y directions. To prevent unphysical boundary reflections, a mask function $M = \cos^{1/6}(\frac{\pi}{2}\frac{R-R_0}{R_{\max}-R_0})$ is applied to the wave function once the internuclear distance exceeds $R_0 = 30$ a.u.

We employ the virtual detector approach [65–71] for efficient backpropagation analysis, eliminating the requirement for extended spatial grids. When the outgoing wave function reaches a virtual detector positioned at $\boldsymbol{R} = \boldsymbol{R}_d$, the probability flux is recorded as

$$\boldsymbol{j}(\boldsymbol{R}_d, t) = \frac{i}{2}\chi_-(\boldsymbol{R}_d, t)\nabla\chi_-^*(\boldsymbol{R}_d, t) + \text{c.c.}, \tag{10}$$

where c.c. denotes the complex conjugate of the preceding term. The local momentum is derived from the phase gradient:

$$\boldsymbol{P}(\boldsymbol{R}_d, t) = \nabla \arg \chi_-(\boldsymbol{R}_d, t). \tag{11}$$

We identify the tunnel exit by propagating the classical trajectories backward in time within the field-dressed potential energy surface V_- of H_2^+.

III. RESULTS AND DISCUSSION

Inspired by the Keldysh parameter [72] for electrons in tunneling ionization, Paci and Wardlaw [42] introduced an analogous parameter for molecular dissociation to distinguish between tunneling dissociation and multiphoton dissociation. The nuclear Keldysh parameter is defined as $\gamma_n = \sqrt{D_p/2U_{pn}}$, where D_p is the dissociation energy and U_{pn} is the ponderomotive energy of the nucleus. A value of $\gamma_n < 1$ corresponds to tunneling dissociation, while $\gamma_n > 1$ indicates multiphoton dissociation.

For H_2^+ in the rovibrational ground state irradiated by a typical Ti:sapphire laser (800 nm central wavelength), achieving $\gamma_n < 1$ to facilitate tunneling dissociation requires a laser intensity of 8×10^{16} W/cm^2. However, at such high intensities, H_2^+ would undergo complete ionization, suppressing the dissociation process. To mitigate ionization and observe tunneling dissociation dynamics, we employ terahertz lasers with wavelengths spanning 50–100 μm, with a peak intensity of 1.3×10^{14} W/cm^2 and a total optical cycle of $N = 2$. Under these conditions, γ_n remains below 1, ensuring the dynamics is unequivocally within the tunneling dissociation regime. The model's accuracy is confirmed by its agreement with experiments at intensities up to 6×10^{14} W/cm^2 [53–55].

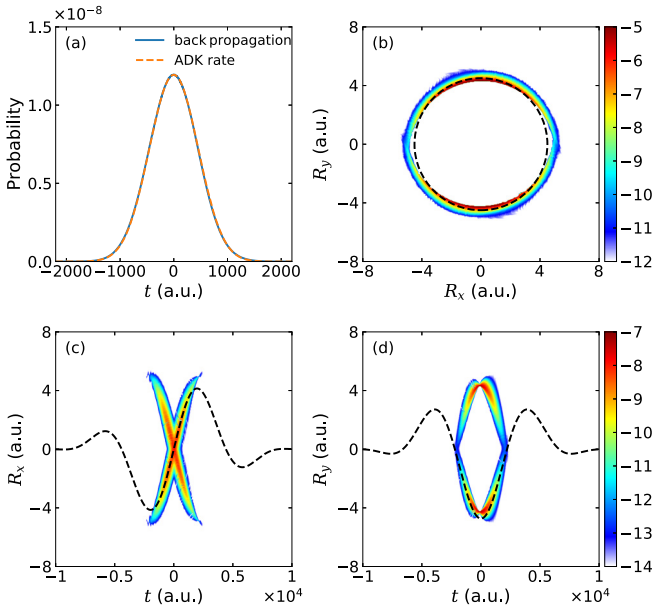

FIG. 2. Distribution of (a) tunneling dissociation time, with ADK rates calculated following Ref. [48], and (b) tunneling exit position. Also shown is the time-resolved distribution of tunneling exit position in the (c) x and (d) y directions. A two-cycle circular laser pulse with a central wavelength of 80 μm and a peak intensity of 1.3×10^{14} W/cm^2 is applied. The black dashed lines denote (b) a circle of radius $R \approx 4.5$ a.u., (c) the x component, and (d) the y component of the electric field (in arbitrary units).

We systematically investigate the tunneling dissociation process using the backpropagation method. A virtual detector positioned at $\boldsymbol{R}_d = 20$ a.u. recorded the probability flux and momentum distributions according to Eqs. (10) and (11). Results obtained with detector positions of 15 and 25 a.u. confirmed that our conclusions remain independent of the specific detector location.

As shown in Fig. 2(a), the calculated temporal distribution of tunneling dissociation, using a laser pulse with a central wavelength of $\lambda = 80$ μm, shows excellent agreement with theoretical predictions from Ref. [48]. Analysis of the spatial distribution [Fig. 2(b)] reveals that the tunneling exit positions are predominantly localized on a characteristic circle with an internuclear distance of $R \approx 4.5$ a.u., marked by the black dashed line. Time-resolved analysis [Figs. 2(c) and 2(d)] shows that the tunneling probability peaks concurrently with the electric-field maximum, while spatial symmetry is maintained throughout the process (see also Fig. 1). However, this symmetry is broken in heteronuclear molecules (HD^+ and HT^+) [50]. These spatiotemporal-resolved quantitative results offer key insights into the strong-field tunneling dissociation mechanism and establish a theoretical foundation for the active control of molecular dissociation.

To elucidate the influence of transitions between $\chi_\pm(\boldsymbol{R}, t)$ states, we implement the single-level approximation, restricting the dynamics to the V_- potential energy surface. This restriction prevents population transfer between the $\chi_+(\boldsymbol{R}, t)$ and $\chi_-(\boldsymbol{R}, t)$ states. Since the V_+ and V_- surfaces yield

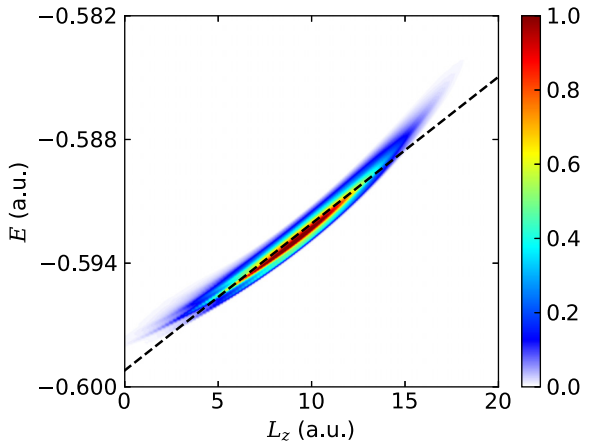

FIG. 3. Correlated spectrum of angular momentum and energy of the proton at the tunnel exit during dissociation of H_2^+. A two-cycle circular laser pulse with a central wavelength of 80 μm and a peak intensity of 1.3×10^{14} W/cm^2 is applied. The black dashed line denotes the conservation law $E = \omega L_z - D_p$ [Eq. (12)].

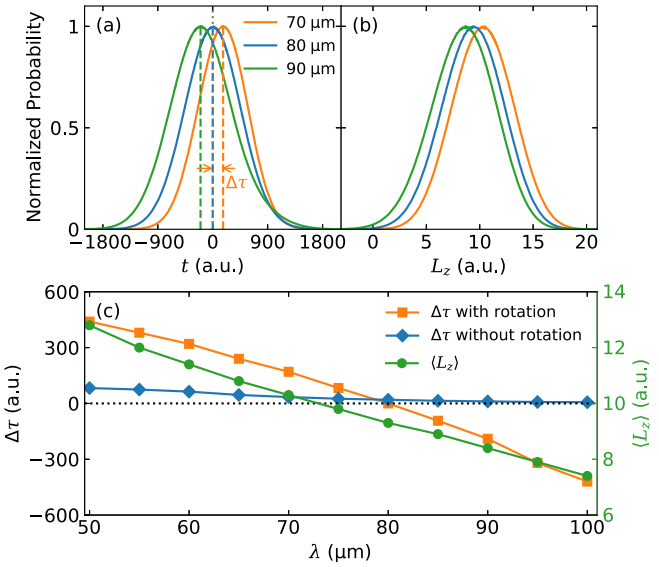

FIG. 4. Distribution of (a) tunneling dissociation time and (b) angular momentum at the tunnel exit for three characteristic wavelengths: 70, 80, and 90 μm. (c) Wavelength dependence of the tunneling time delay $\Delta\tau$ and the mean angular momentum $\langle L_z \rangle$. A two-cycle circular laser pulse with a peak intensity of 1.3×10^{14} W/cm^2 is applied.

comparable dissociation probabilities, confining the dynamics to V_- alone approximately doubles the dissociation yield compared to the full dynamical model, where nonadiabatic population redistribution is allowed. Nevertheless, the essential physical conclusions regarding temporal distributions and exit positions remain fully consistent, demonstrating that transitions between $\chi_\pm(\boldsymbol{R}, t)$ states have negligible impact on the extracted tunneling exit information.

To provide a complete characterization of the tunneling exit dynamics and to establish the universality of fundamental laws in strong-field processes, we extend the recently discovered concept of the subcycle conservation law from the atomic to the molecular domain. Under circular light, the system possesses an infinite-order continuous dynamical symmetry, which leads to a conservation law between angular momentum and energy that holds down to the subcycle level. This law, characterized by a correlated spectrum of angular momentum and energy (SAME), has been demonstrated previously for photoelectrons in atomic tunneling ionization [73,74]. Here we demonstrate that this fundamental concept can be generalized to molecular tunneling dissociation. Applying the backpropagation method, we compute the SAME distribution for protons at the tunnel exit (Fig. 3). Our calculations reveal a pronounced linear relationship between the proton angular momentum L_z and its energy E, given by

$$E = \omega L_z - D_p. \tag{12}$$

This conservation law dictates that for each photon absorbed during the under-barrier tunneling dissociation process, the proton simultaneously acquires a quantum of angular momentum and a quantum of photon energy. This result successfully generalizes the subcycle conservation law from electronic ionization in atoms to nuclear dissociation in molecules and establishes the universality of this fundamental correlation in strong-field tunneling processes. It provides fundamental conservation-law-level support for the efficient field-mediated transfer of angular momentum and kinetic energy to the dissociating protons. This conservation directly underpins the central mechanism to be identified in this work that the field-driven rotation of the molecule actively modulates the tunneling dynamics.

Having established the spatiotemporal characteristics of the tunneling dissociation process, we proceed to investigate how the dissociation time delay is modulated by the laser parameters. The tunneling dissociation time delay $\Delta\tau$ is defined as the difference between the time at which the tunneling dissociation probability is maximized in a specific dissociation channel, e.g., via the V_- surface, and the time of the peak electric field of the driving THz pulse, which is set as $t = 0$. To isolate the effect of pulse duration, we perform calculations with a fixed laser intensity of 1.3×10^{14} W/cm^2 and a two-cycle pulse, varying only the wavelength. The resulting tunneling dissociation time distributions for wavelengths of 70, 80, and 90 μm are presented in Fig. 4(a). For the 80-μm pulse, the tunneling probability peaks at the pulse center, exhibiting no significant delay. In contrast, reducing the wavelength to 70 μm shifts the distribution peak to later times, indicating a positive delay. Conversely, increasing the wavelength to 90 μm causes a clear advance of the distribution peak, resulting in a negative delay.

The dependence of the tunneling dissociation time delay $\Delta\tau$ on the laser wavelength, accounting for molecular rotation, is displayed as the yellow curve in Fig. 4(c). The curve reveals two distinct regimes. For wavelengths below 80 μm, the delay is positive and decreases monotonically as the wavelength increases. In contrast, for wavelengths above 80 μm, the delay becomes negative and its magnitude grows progressively. This systematic transition demonstrates a clear and strong correlation between the tunneling dissociation time delay and the laser wavelength.

The observed wavelength dependence of the time delay underscores the pivotal role of molecular rotation. Although vibrational and rotational motions are traditionally treated separately, incorporating molecular rotation as a dynamic degree of freedom is often essential in strong-field molecular physics. This is particularly evident in the midinfrared laser-induced dissociation of H_2^+, where the laser field efficiently drives rotational excitation via the induced dipole moment, a phenomenon supported by experiments [75,76] and theoretical simulations [56]. A key factor is the comparable timescale between the laser optical cycle (0.17–0.34 ps for 50–100 μm wavelengths) and the rotational period of H_2^+ (approximately equal to 0.5 ps) [77]. This temporal matching elevates rotational effects from a negligible perturbation to a dominant mechanism governing dissociation dynamics [50]. At 80 μm, the laser optical cycle equals half the rotational period, establishing a resonant condition: When the laser field peaks, the outgoing nuclear wave packet aligns precisely with the electric-field direction, ultimately yielding a vanishing time delay.

To elucidate the physical mechanism underlying the correlation between the tunneling dissociation time delay and the laser wavelength, we analyze the mean angular momentum distribution at the tunnel exit for wavelengths of 70, 80, and 90 μm [Fig. 4(b)]. A clear correlation emerges: A significant negative delay at 90 μm correlates with lower angular momentum, whereas a distinct positive delay at 70 μm is associated with higher angular momentum. This trend demonstrates that an increase in laser frequency leads to a marked rise in angular momentum at the tunnel exit, signifying an enhanced molecular rotational speed. Crucially, the wavelength dependence of the mean angular momentum $\langle L_z \rangle$ [Fig. 4(c), green curve] not only exhibits a negative correlation with the wavelength but also precisely mirrors the tunneling time delay. This agreement provides robust evidence that the observed tunneling dissociation time delay is intrinsically governed by laser-driven molecular rotational dynamics.

To verify the pivotal role of molecular rotation, we construct a simplified model that restricts rotation and considers only vibrational degrees of freedom, following the spirit of earlier light-induced potential studies [57]. The TDSE for this model is given by

$$i\frac{\partial}{\partial t}\begin{pmatrix}\chi_g(R,\theta,t)\\ \chi_u(R,\theta,t)\end{pmatrix} = (H_0 + H_I)\begin{pmatrix}\chi_g(R,\theta,t)\\ \chi_u(R,\theta,t)\end{pmatrix}, \tag{13}$$

where the field-free Hamiltonian H_0 is defined as

$$H_0 = \begin{pmatrix}\frac{P_R^2}{2\mu} + V_g(R,\theta) & 0\\ 0 & \frac{P_R^2}{2\mu} + V_u(R,\theta)\end{pmatrix}. \tag{14}$$

Here the angle θ between the molecular orientation and laser polarization axis is now treated as a fixed parameter rather than a dynamical variable. The interaction Hamiltonian is given by

$$H_I = \begin{pmatrix}0 & M(R,\theta,t)\\ M(R,\theta,t) & 0\end{pmatrix}, \tag{15}$$

where $M(R,\theta,t) = F_x(t)D(R)\cos\theta + F_y(t)D(R)\sin\theta$.

Within this model, the presented rotationless results are computed by synthesizing the tunneling time distributions from 2000 independent TDSE solutions, each corresponding to a uniformly spaced θ value in $[0, 2\pi)$. This procedure represents an isotropically oriented, nonrotating ensemble.

The results from the vibration-only model provide a critical baseline for comparison. As shown by the blue curve in Fig. 4(c), the tunneling time delay in the absence of molecular rotation exhibits a markedly different dependence on laser wavelength. As the wavelength increases (corresponding to longer pulse durations), the delay decreases monotonically toward zero. The mechanism behind the tunneling dissociation time delay lies in the timescale matching between the laser pulse and the nuclear-wave-packet dynamics. When the laser pulse duration is sufficiently long, the nuclear wave packet has ample time to adapt to the changes in the external field, driving the process into the adiabatic regime where the tunneling delay approaches zero. Conversely, when the pulse duration is short, the nuclear wave packet cannot respond promptly to the external field variations, causing the process to enter the nonadiabatic regime, where a significant delay is observed. The contrast between results with and without rotation conclusively identifies molecular rotation as a key mechanism modulating the tunneling dissociation time delay.

Our results offer a clear physical picture for the wavelength-dependent tunneling delay. The sign of the delay, positive below 80 μm and negative above, is largely determined by the competition between the relative timescales between laser cycle and molecular rotational period. At 80 μm, these timescales match, leading to phase-locked rotation and a negligible net delay. At 90 μm, the laser field rotates more slowly than the molecule; this allows the molecule to prealign with the field, causing tunneling to occur before the field maximum and producing a negative delay. Conversely, at 70 μm, the laser field rotates faster, causing the molecular axis to lag behind; this delays the tunneling event until after the peak field, resulting in a positive delay.

To provide quantitative support for this rotational modulation mechanism, we analyze the time-dependent average orientation $\langle\theta(t)\rangle$ of the nuclear wave packet under different wavelengths. The angle θ is defined relative to the y axis and the instantaneous field direction is aligned with the $\theta = 0$ direction at the field peak ($t = 0$). As shown in Fig. 5, at 70 μm, $\langle\theta(0)\rangle$ remains consistently below 0 around the peak field time ($t = 0$), indicating that the wave packet is biased toward quadrants I and III. This angular lag results in the tunneling probability maximum occurring after the field peak, corresponding to a positive delay. At 90 μm, $\langle\theta(0)\rangle$ stays above 0, reflecting a concentration of the wave packet in quadrants II and IV. This alignment leads to tunneling before the field peak and a negative delay. At 80 μm, $\langle\theta(0)\rangle$ is close to 0, demonstrating that the wave packet is nearly aligned with the instantaneous field direction, which results in synchronized tunneling and a near-zero net delay. These observations quantitatively link the dynamic angular offset between the molecular axis and the rotating field to the sign and magnitude of the measured delay. This mechanism demonstrates how tunneling time delay can serve as a real-time probe of molecular rotation, capturing the subtle interplay between field-driven rotational dynamics and the timing of the tunneling process.

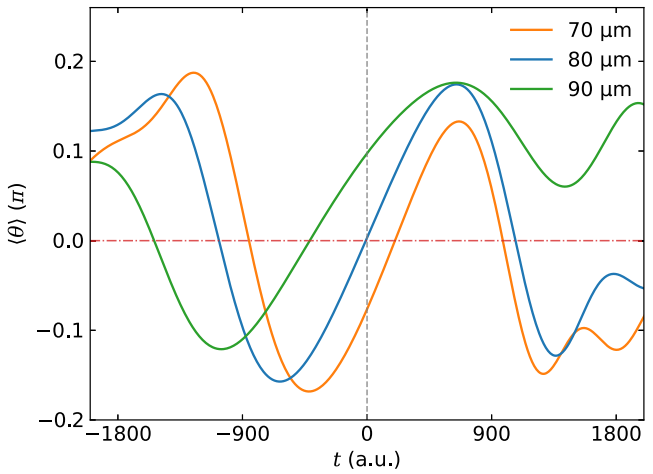

FIG. 5. Temporal evolution of the average orientation angle $\langle\theta(t)\rangle$ of the nuclear wave packet for three characteristic wavelengths: 70, 80, and 90 μm. The time $t = 0$ marks the peak of the laser pulse (gray dashed line), when the electric field points along the y axis ($\theta = 0$). The laser parameters are the same as in Fig. 4.

IV. CONCLUSION

We have investigated the full quantum dynamics of tunneling dissociation of H_2^+ in circularly polarized terahertz laser fields by numerically solving a two-level time-dependent Schrödinger equation. By extending the backpropagation method from atomic ionization to molecular dissociation, we have characterized key ultrafast dynamical characteristics, including the dissociation time delay, exit position, and momentum distribution, providing a complete spatiotemporal picture of the tunneling dissociation process. Our results reveal a strong correlation between the tunneling dissociation time delay and the relative timescale between the laser field period and molecular rotation: A near-zero delay occurs at matched periods, negative delays emerge when the laser period exceeds half the rotational period, and positive delays appear in the opposite regime. These findings establish tunneling time delays as a sensitive probe of ultrafast molecular rotational dynamics. This work not only deepens the understanding of laser-molecule interactions but also opens a route toward controlling molecular dissociation through rotational synchronization, thereby advancing the toolkit for studying ultrafast molecular dynamics with strong-field techniques.

ACKNOWLEDGMENTS

This work was supported by the Quantum Science and Technology–National Science and Technology Major Project (Grant No. 2024ZD0300700), the National Natural Science Foundation of China (Grants No. 12304379, No. 12474341, No. 12521003, No. 12227807, No. 12241407, and No. 12274294), the Educational Department of Liaoning Province (Grant No. LJKMZ20220442), the Science and Technology Commission of Shanghai Municipality (Grants No. 23JC1402000 and No. 24YF2710000), and the Shanghai Pilot Program for Basic Research (Grant No. TQ20240204). Numerical computations were in part performed on the ECNU Multifunctional Platform for Innovation (001).

DATA AVAILABILITY

The data that support the findings of this article are openly available [78].

[1] L. A. MacColl, Note on the transmission and reflection of wave packets by potential barriers, Phys. Rev. **40**, 621 (1932).
[2] R. Landauer and T. Martin, Barrier interaction time in tunneling, Rev. Mod. Phys. **66**, 217 (1994).
[3] A. S. Landsman and U. Keller, Attosecond science and the tunnelling time problem, Phys. Rep. **547**, 1 (2015).
[4] C. Hofmann, A. S. Landsman, and U. Keller, Attoclock revisited on electron tunnelling time, J. Mod. Opt. **66**, 1052 (2019).
[5] A. S. Kheifets, The attoclock and the tunneling time debate, J. Phys. B **53**, 072001 (2020).
[6] C. Hofmann, A. Bray, W. Koch, H. Ni, and N. I. Shvetsov-Shilovski, Quantum battles in attoscience: Tunnelling, Eur. Phys. J. D **75**, 208 (2021).
[7] Y. Ma, H. Ni, and J. Wu, Attosecond ionization time delays in strong-field physics, Chin. Phys. B **33**, 013201 (2024).
[8] P. Eckle, M. Smolarski, P. Schlup, J. Biegert, A. Staudte, M. Schöffler, H. G. Muller, R. Dörner, and U. Keller, Attosecond angular streaking, Nat. Phys. **4**, 565 (2008).
[9] P. Eckle, A. N. Pfeiffer, C. Cirelli, A. Staudte, R. Dörner, H. G. Muller, M. Büttiker, and U. Keller, Attosecond ionization and tunneling delay time measurements in helium, Science **322**, 1525 (2008).
[10] A. N. Pfeiffer, C. Cirelli, M. Smolarski, D. Dimitrovski, M. Abu-samha, L. B. Madsen, and U. Keller, Attoclock reveals natural coordinates of the laser-induced tunnelling current flow in atoms, Nat. Phys. **8**, 76 (2012).
[11] L. Torlina, F. Morales, J. Kaushal, I. Ivanov, A. Kheifets, A. Zielinski, A. Scrinzi, H. G. Muller, S. Sukiasyan, M. Ivanov, and O. Smirnova, Interpreting attoclock measurements of tunnelling times, Nat. Phys. **11**, 503 (2015).
[12] H. Ni, U. Saalmann, and J.-M. Rost, Tunneling ionization time resolved by backpropagation, Phys. Rev. Lett. **117**, 023002 (2016).
[13] N. Eicke and M. Lein, Trajectory-free ionization times in strong-field ionization, Phys. Rev. A **97**, 031402 (2018).
[14] M. Klaiber, K. Z. Hatsagortsyan, and C. H. Keitel, Under-the-tunneling-barrier recollisions in strong-field ionization, Phys. Rev. Lett. **120**, 013201 (2018).
[15] A. W. Bray, S. Eckart, and A. S. Kheifets, Keldysh-Rutherford model for the attoclock, Phys. Rev. Lett. **121**, 123201 (2018).
[16] W. Quan, V. V. Serov, M. Wei, M. Zhao, Y. Zhou, Y. Wang, X. Lai, A. S. Kheifets, and X. Liu, Attosecond molecular angular streaking with all-ionic fragments detection, Phys. Rev. Lett. **123**, 223204 (2019).

[17] U. S. Sainadh, H. Xu, X. Wang, A. Atia-Tul-Noor, W. C. Wallace, N. Douguet, A. Bray, I. Ivanov, K. Bartschat, A. Kheifets, R. T. Sang, and I. V. Litvinyuk, Attosecond angular streaking and tunnelling time in atomic hydrogen, Nature (London) **568**, 75 (2019).

[18] M. Yu, K. Liu, M. Li, J. Yan, C. Cao, J. Tan, J. Liang, K. Guo, W. Cao, P. Lan, Q. Zhang, Y. Zhou, and P. Lu, Full experimental determination of tunneling time with attosecond-scale streaking method, Light: Sci. Appl. **11**, 215 (2022).

[19] M. Klaiber, Q. Z. Lv, S. Sukiasyan, D. Bakucz Canário, K. Z. Hatsagortsyan, and C. H. Keitel, Reconciling conflicting approaches for the tunneling time delay in strong field ionization, Phys. Rev. Lett. **129**, 203201 (2022).

[20] M. Klaiber, D. Bakucz Canário, and K. Z. Hatsagortsyan, Sub-barrier recollisions and the three classes of tunneling time delays in strong-field ionization, Phys. Rev. A **107**, 053103 (2023).

[21] S. Landsman, M. Weger, J. Maurer, R. Boge, A. Ludwig, S. Heuser, C. Cirelli, L. Gallmann, and U. Keller, Ultrafast resolution of tunneling delay time, Optica **1**, 343 (2014).

[22] G. Orlando, C. R. McDonald, N. H. Protik, G. Vampa, and T. Brabec, Tunnelling time, what does it mean? J. Phys. B **47**, 204002 (2014).

[23] T. Zimmermann, S. Mishra, B. R. Doran, D. F. Gordon, and A. S. Landsman, Tunneling time and weak measurement in strong field ionization, Phys. Rev. Lett. **116**, 233603 (2016).

[24] N. Teeny, E. Yakaboylu, H. Bauke, and C. H. Keitel, Ionization time and exit momentum in strong-field tunnel ionization, Phys. Rev. Lett. **116**, 063003 (2016).

[25] N. Camus, E. Yakaboylu, L. Fechner, M. Klaiber, M. Laux, Y. Mi, K. Z. Hatsagortsyan, T. Pfeifer, C. H. Keitel, and R. Moshammer, Experimental evidence for quantum tunneling time, Phys. Rev. Lett. **119**, 023201 (2017).

[26] N. Douguet and K. Bartschat, Dynamics of tunneling ionization using Bohmian mechanics, Phys. Rev. A **97**, 013402 (2018).

[27] M. Yuan, Direct probing of tunneling time in strong-field ionization processes by time-dependent wave packets, Opt. Express **27**, 6502 (2019).

[28] R. Ramos, D. Spierings, I. Racicot, and A. M. Steinberg, Measurement of the time spent by a tunnelling atom within the barrier region, Nature (London) **583**, 529 (2020).

[29] G. Çelebi, E. Özçelik, E. Vardar, and D. Demir, Time delay during the proton tunneling in the base pairs of the DNA double helix, Prog. Biophys. Mol. Biol. **167**, 96 (2021).

[30] E. Özçelik, D. E. Akar, S. Zaman, and D. Demir, Time delay during intra-base proton tunneling in the guanine base of the single stranded DNA, Prog. Biophys. Mol. Biol. **173**, 4 (2022).

[31] P. R. Schreiner, H. P. Reisenauer, F. C. Pickard IV, A. C. Simmonett, W. D. Allen, E. Mátyus, and A. G. Császár, Capture of hydroxymethylene and its fast disappearance through tunnelling, Nature (London) **453**, 906 (2008).

[32] P. R. Schreiner, Tunneling control of chemical reactions: The third reactivity paradigm, J. Am. Chem. Soc. **139**, 15276 (2017).

[33] T. Constantin, B. Górski, M. J. Tilby, S. Chelli, F. Juliá, J. Llaveria, K. J. Gillen, H. Zipse, S. Lakhdar, and D. Leonori, Halogen-atom and group transfer reactivity enabled by hydrogen tunneling, Science **377**, 1323 (2022).

[34] P. H. Bucksbaum, A. Zavriyev, H. G. Muller, and D. W. Schumacher, Softening of the H_2^+ molecular bond in intense laser fields, Phys. Rev. Lett. **64**, 1883 (1990).

[35] G. Yao and S.-I. Chu, Molecular-bond hardening and dynamics of molecular stabilization and trapping in intense laser pulses, Phys. Rev. A **48**, 485 (1993).

[36] A. Giusti-Suzor, X. He, O. Atabek, and F. H. Mies, Above-threshold dissociation of H_2^+ in intense laser fields, Phys. Rev. Lett. **64**, 515 (1990).

[37] Z.-C. Li and F. He, *Ab initio* non-Born-Oppenheimer simulations of rescattering dissociation of H_2 in strong infrared laser fields, Phys. Rev. A **90**, 053423 (2014).

[38] Z.-C. Li, C. Ruiz, and F. He, Tunneling dissociation of H_2^+ and its isotopes in THz laser pulses, Phys. Rev. A **90**, 033421 (2014).

[39] O. I. Tolstikhin, H. J. Wörner, and T. Morishita, Effect of nuclear motion on tunneling ionization rates of molecules, Phys. Rev. A **87**, 041401 (2013).

[40] X. Wang, H. Xu, A. Atia-Tul-Noor, B. T. Hu, D. Kielpinski, R. T. Sang, and I. V. Litvinyuk, Isotope effect in tunneling ionization of neutral hydrogen molecules, Phys. Rev. Lett. **117**, 083003 (2016).

[41] M. Thachuk and D. M. Wardlaw, Classical analysis of diatomic dissociation dynamics in intense laser fields, J. Chem. Phys. **102**, 7462 (1995).

[42] J. T. Paci and D. M. Wardlaw, The dissociation adiabaticity parameter and the strong field dissociation of H_2^+, J. Chem. Phys. **119**, 7824 (2003).

[43] F. Châteauneuf, T.-T. Nguyen-Dang, N. Ouellet, and O. Atabek, Multiphoton dissociation of H_2^+ in intense laser fields: Field-dressed-propagator method, J. Chem. Phys. **108**, 3974 (1998).

[44] H. Abou-Rachid, T. T. Nguyen-Dang, and O. Atabek, Multiphoton dissociation of H_2^+ in intense laser fields: A dynamical study of the interplay between direct and sequential mechanisms, J. Chem. Phys. **110**, 4737 (1999).

[45] H. Abou-Rachid, T. T. Nguyen-Dang, and O. Atabek, Dynamical quenching of the dissociation of H_2^+ in intense laser fields, J. Chem. Phys. **114**, 2197 (2001).

[46] H. Niikura, P. B. Corkum, and D. M. Villeneuve, Mapping attosecond electron wave packet motion, Phys. Rev. Lett. **90**, 203601 (2003).

[47] F. Kelkensberg, C. Lefebvre, W. Siu, O. Ghafur, T. T. Nguyen-Dang, O. Atabek, A. Keller, V. Serov, P. Johnsson, M. Swoboda, T. Remetter, A. L'Huillier, S. Zherebtsov, G. Sansone, E. Benedetti, F. Ferrari, M. Nisoli, F. Lépine, M. F. Kling, and M. J. J. Vrakking, Molecular dissociative ionization and wave-packet dynamics studied using two-color XUV and IR pump-probe spectroscopy, Phys. Rev. Lett. **103**, 123005 (2009).

[48] S. Chelkowski, A. D. Bandrauk, and P. B. Corkum, Muonic molecules in superintense laser fields, Phys. Rev. Lett. **93**, 083602 (2004).

[49] R. Zhang, J. Chen, S. Yan, W. Jie, and C. Ning, Photodetachment and tunneling dissociation of cryogenic double Rydberg anions NH_4^+, J. Phys. Chem. Lett. **15**, 5612 (2024).

[50] Y. D. Tian, K. L. Liu, Y. C. Wang, Y. M. Zhou, and P. X. Lu, Proton tunneling in the dissociation of H_2^+ and its asymmetric isotopologues driven by circularly polarized THz laser pulses, J. Chem. Phys. **160**, 114311 (2024).

[51] H. Ni, U. Saalmann, and J.-M. Rost, Tunneling exit characteristics from classical backpropagation of an ionized electron wave packet, Phys. Rev. A **97**, 013426 (2018).

[52] H. Ni, N. Eicke, C. Ruiz, J. Cai, F. Oppermann, N. I. Shvetsov-Shilovski, and L.-W. Pi, Tunneling criteria and a nonadiabatic term for strong-field ionization, Phys. Rev. A **98**, 013411 (2018).

[53] M. F. Kling, C. Siedschlag, A. J. Verhoef, *et al.*, Control of electron localization in molecular dissociation, Science **312**, 246 (2006).

[54] M. Kremer, B. Fischer, B. Feuerstein, V. L. B. de Jesus, V. Sharma, C. Hofrichter, A. Rudenko, U. Thumm, C. D. Schröter, R. Moshammer, and J. Ullrich, Electron localization in molecular fragmentation of H_2 by carrier-envelope phase stabilized laser pulses, Phys. Rev. Lett. **103**, 213003 (2009).

[55] H. Xu, T. Y. Xu, F. He, D. Kielpinski, R. T. Sang, and I. V. Litvinyuk, Momentum spectra for tunneling ionization of Xe in intense laser pulses: Comparison between theory and experiment, Phys. Rev. A **89**, 041403 (2014).

[56] L. Xu and F. He, Electron-localization-resolved rotation of D_2^+ in a strong midinfrared laser pulse, Phys. Rev. A **102**, 023106 (2020).

[57] M. Kübel, M. Spanner, Z. Dube, A. Y. Naumov, S. Chelkowski, A. D. Bandrauk, M. J. J. Vrakking, P. B. Corkum, D. M. Villeneuve, and A. Staudte, Probing multiphoton light-induced molecular potentials, Nat. Commun. **11**, 2596 (2020).

[58] Z. Chen, P.-L. He, and F. He, Spiral nuclear momentum distribution for the dissociation of H_2^+ in a circularly polarized laser pulse, Phys. Rev. A **101**, 033406 (2020).

[59] Z. Chen and F. He, Interference of nuclear wave packets carrying different angular momenta in the dissociation of H_2^+ in strong circularly polarized laser pulses, Phys. Rev. A **102**, 033107 (2020).

[60] T. E. Sharp, Potential-energy curves for molecular hydrogen and its ions, At. Data Nucl. Data Tables **2**, 119 (1970).

[61] D. E. Ramaker and J. M. Peek, Critical assessment of the electronic-energy terms of the hydrogen molecular ion, At. Data Nucl. Data Tables **5**, 167 (1973).

[62] T. Y. Xu and F. He, Dissociation of D_2^+ by UV and THz light pulses, Phys. Rev. A **88**, 043426 (2013).

[63] R. Kosloff and D. Kosloff, Absorbing boundaries for wave propagation problems, J. Comput. Phys. **63**, 363 (1986).

[64] J. Wang, C. Zhang, Y. Li, and Y. Ding, Finite difference method for solving one-dimensional nonlinear harmonic oscillator problems, J. Liaoning Univ. (Nat. Sci. Ed.) **50**, 154 (2023).

[65] B. Feuerstein and U. Thumm, On the computation of momentum distributions within wavepacket propagation calculations, J. Phys. B **36**, 707 (2003).

[66] X. Wang, J. Tian, and J. H. Eberly, Extended virtual detector theory for strong-field atomic ionization, Phys. Rev. Lett. **110**, 243001 (2013).

[67] X. Wang, J. Tian, and J. Eberly, Virtual detector theory for strong-field atomic ionization, J. Phys. B **51**, 084002 (2018).

[68] R.-H. Xu and X. Wang, Extended virtual detector theory including quantum interferences, AIP Adv. **11**, 025124 (2021).

[69] N. Teeny, C. H. Keitel, and H. Bauke, Virtual-detector approach to tunnel ionization and tunneling times, Phys. Rev. A **94**, 022104 (2016).

[70] J.-P. Wang and F. He, Tunneling ionization of neon atoms carrying different orbital angular momenta in strong laser fields, Phys. Rev. A **95**, 043420 (2017).

[71] D. Younis and J. H. Eberly, Strong-field nonsequential double photoionization using virtual-detector theory with path summation, Phys. Rev. A **107**, 053117 (2023).

[72] L. V. Keldysh, Ionization in the field of a strong electromagnetic wave, Zh. Eksp. Teor. Fiz. **47**, 1945 (1964) [Sov. Phys. JETP **20**, 1307 (1965)].

[73] Y. Ma, H. Ni, Y. Li, F. He, and J. Wu, Subcycle angular momentum-energy correlation in atomic tunneling ionization, Ultrafast Sci. **4**, 0071 (2024).

[74] J. Dubois, C. Lévêque, J. Caillat, R. Taïeb, U. Saalmann, and J.-M. Rost, Energy conservation law in strong-field photoionization by circularly polarized light, Phys. Rev. A **109**, 013112 (2024).

[75] Y. Shao, P. He, M.-M. Liu, X. Sun, M. Li, Y. Deng, C. Wu, F. He, Q. Gong, and Y. Liu, Fully differential study on dissociative ionization dynamics of deuteron molecules in strong elliptical laser fields, Phys. Rev. A **95**, 031404 (2017).

[76] X. Gong, P. He, J. Ma, W. Zhang, F. Sun, Q. Ji, K. Lin, H. Li, J. Qiang, P. Lu, H. Li, H. Zeng, J. Wu, and F. He, Observation of photon-nucleus angular-momentum transfer in the strong-field breaking of molecules, Phys. Rev. A **99**, 063407 (2019).

[77] F. Anis and B. D. Esry, Role of nuclear rotation in dissociation of H_2^+ in a short laser pulse, Phys. Rev. A **77**, 033416 (2008).

[78] H. Ni, Molecular-rotation-induced modulation of the tunneling dissociation time delay in H_2^+, Zenodo (2026), https://doi.org/10.5281/zenodo.17711249.